PAPER

NJC

www.rsc.org/njc

Evidence for immobilized photo-Fenton degradation of organic compounds on structured silica surfaces involving Fe recycling

Anna Bozzi,[a] Tatiana Yuranova,[a] Jerzy Mielczarski[b] and John Kiwi*[a]

[a] *Laboratory of Photonics and Interfaces, Institute of Molecular Chemistry and Biology, Swiss Federal Institute of Technology, Lausanne 1015, Switzerland*

[b] *Laboratory Environnement et Minéralurgie (CNRS UMR 7569), CNRS INPL-ENSG, BP 40, 5041, Vandoeuvre-lès-Nancy cedex, France*

Received* (in Toulouse, France) *15th September 2003, Accepted 27th November 2003
First published as an Advance Article on the web 4th March 2004

The present study reports on the use of novel structured inorganic silica fabrics loaded with Fe ions by exchange-impregnation as a heterogeneous photocatalyst. These Fe–silica fabrics are denoted EGF/Fe(0.4%). Experimental evidence shows that Fe ions are released from the silica fabrics and react with H_2O_2 to form oxidative radicals in solution; the Fe ions are reduced to Fe(II) during oxalic acid and oxalate oxidation. The Fe^{3+} is extracted from the support to the aqueous medium where it is re-oxidized by being re-adsorbed onto the silica fabric. The contributions of the homogeneous and heterogeneous photocatalysis processes during the degradation of oxalic acid and oxalates were quantified as a function of the solution pH and the results presented agree with the modeling of the iron oxide surface in the presence of oxalates at different pH values. By attenuated total reflection infrared spectroscopy (ATRIR), the asymmetric stretching vibration doublet band at 1740 cm^{-1} and the satellite peaks corresponding to surface carboxylates were followed during the photocatalytic destruction of the oxalates. The results obtained indicate that the oxalate decomposition channel involves a fast light-activated decarboxylation of the Fe complex: $[RCO_2Fe]^{2+} \rightarrow [R^{\bullet}] + CO_2 + Fe^{2+}$. The structural features of the EGF/Fe(0.4%) surfaces were investigated before and after the oxalate photocatalysis by high resolution transmission electron microscopy (HRTEM), X-ray photoelectron spectroscopy (XPS) and gas adsorption studies (BET).

Introduction

Oxidation of organic substances catalyzed by transition metal ions is a topic of great interest in both industrial and biological chemistry. Inorganic membranes and fabrics represent a very promising approach to finding stable, chemically suitable and cost effective interfaces to carry out immobilized Fenton degradation of organic compounds. Inorganic silica fabrics, due to their known amenability to chemical modification, are one of the most promising support materials for Fenton immobilized systems.[1–3] The development of supported Fenton catalysts has over the years become important in the emerging field of advanced oxidation technologies (AOT's)[3–5] since this approach avoids the iron sludge formed by using dark or photo-assisted homogeneous Fenton pre-treatment. Recently, the use of Fenton-like reactions for the treatment of contaminated soil[6] and the subsurface has increased because of the ability of the Fenton reagent to rapidly oxidize and mineralize bio-refractory organic contaminants.[7] The present study shows that the Fe^{2+} ions remaining in solution after oxalic acid degradation go back to the catalyst surface and participate in a new degradation cycle. This is similar to the mechanism for Fenton chemistry suggested for soil and ground water remediation.

The EGF/Fe(0.4%) fabrics presented in this study avoid iron leaching during the photo-induced process. EEC regulations[8] allow only up to 2 ppm of iron ions in drinking water. These EGF/Fe(0.4%) fabrics present acceptable kinetics and resist oxidative radical attack during Fenton processes. In this study we address oxalic acid degradation by focusing on the molecular mechanism of the surface photochemistry on Fe-loaded fabrics because (a) this compound and formic acid are probably the last produced during the abatement of organic compounds before being finally mineralized to CO_2 and (b) oxalic acid and oxalates are essentially unreactive to attack by OH radicals.[2,4,5] The ferrioxalate system has been studied in a homogeneous solution as an actinometer[9,10] and in biological systems.

It is our intention to probe the molecular mechanism taking place on the EGF/Fe(0.4%) fabric surface and establish (a) the photo-reduction kinetics of the complex $[Fe(III)(Ox)_{n=1-3}]^{\delta-}$, (b) the formation of iron carboxylate during the photo-degradation process and (c) the reaction mechanism of oxalic acid degradation. By modeling the surface of Fe_2O_3 and the ionization of oxalate in solution the interaction between oxalic acid and the EGF/Fe(0.4%) fabric during oxalic acid and oxalate oxidation will be determined.

Experimental

Materials

Oxalic acid, H_2O_2, HCl, $FeCl_3 \cdot 6H_2O$, Ferro-Zine® and hydroxylamine hydrocloride were Fluka p.a. reagents and used as received. Triply distilled water was used in all experiments.

Preparation of supported Fe–silica fabrics. Following a recently reported procedure,[2,3] alumino-borosilicate fibers (EGF fabric, where EGF stands for extruded glass fabrics), obtained from Vetrotex and containing SiO_2, B_2O_3, MgO, Al_2O_3, K_2O, Na_2O, Fe_2O_3, were treated with HCl to leach out all the non-silica components. The iron loading on the silica fabrics was obtained by ion exchange from an aqueous solution of Mohr's salt, $Fe(NH_4)_2(SO_4)_2 \cdot 6H_2O$. The fabrics were dried at 80 °C and calcined at 450 °C for 1 h. The samples were rinsed with distilled water and dried in air at 50 °C.

DOI: 10.1039/b316027k

Methods

Photo-reactor and irradiation procedures. The photocatalytic activity of the structured Fe–silica fabrics was evaluated in cylindrical Pyrex flasks each containing 70 ml of reagent solution. The Fe–SiO_2 fabric catalyst strips of 48 cm^2 were immediately placed behind the wall of the reaction vessel. Irradiation of the vessels was carried out inside the cavity of a Hanau Suntest solar simulator having an intensity of 90 mW cm^{-2}.

Analysis of the irradiated solutions. Spectrophotometric analyses of the solutions were carried out by a Hewlett–Packard 8452 diode array spectrophotometer. The total organic carbon (TOC) was monitored *via* a Shimadzu 500 instrument equipped with an ASI automatic sample injector. The peroxide concentrations were assessed by Merkoquant paper® at levels between 0.5 and 25 mg l^{-1} of H_2O_2. The total iron concentration in the irradiated solutions was measured by complexation with Ferro-Zine® (Aldrich16,060-1) in the presence of hydroxylamine hydrochloride.

Ion chromatography. The quantitative determination of oxalic acid was carried out by ion chromatography using a Dionex 4000i (Dionex, Sunnyvale, CA, USA) LC system working in suppressed ion mode and equipped with a conductivity detector. Samples, injected *via* a 50 ml loop, were eluted at a flow rate of 1 ml min^{-1} through an OmniPac PAX-500 analytical column.

ATRIR spectroscopy. Attenuated total reflection infrared spectroscopy (ATRIR) was applied to the study of the structured Fe–silica surfaces. The reflection spectra were recorded on a Bruker IFS 55 FTIR spectrophotometer equipped with a calcium telluride detector and an internal reflection attachment from Harrick Co. A detailed description of the applied ATR technique can be found in reference.[11]

Transmission electron microscopy and energy dispersive X-ray spectrometry (EDX). Transmission electron microscopy (TEM) was performed on a Philips CM 300UT/FEG microscope fitted with a Schottky field emission gun. Thin TEM foils were prepared by cryo-ultramicroscopy. Small pieces of the sample were embedded in epoxy and cut at liquid nitrogen temperature with a Diatome diamond knife with a 45° cutting edge. Chemical analysis was performed by energy dispersive X-ray spectrometry (EDX) with an organic detector window. Selected area electron diffraction (SAED) was then considered as a convenient tool for the analysis of the samples. The ring patterns superimposed on an intense background showed a contrast that was sufficient for accurate phase determination.

Gas adsorption studies. Physisorption was carried out using a Sorptomatic 1900 Micropore unit. A precision of 2% was attained in the reproducibility of the adsorption isotherms. The experiments were performed at the liquid nitrogen boiling temperature of 77 K.

X-Ray photoelectron spectroscopy (XPS). Experiments were performed with a Leybold–Heraeus instrument (LHS 12) using MgK_α radiation at a power of 200 W. The binding energies of the peaks were referenced to the Au 4 $f_{7/2}$ energy level of 84 eV. The standard Shirley[12] treatment was used for the quantitative evaluation of the background correction. Electrostatic charging effects were referenced by calibration to the C1s signal.

Modeling

The Acuchem program (NIST, Gaithersburg, MD) was used for modeling the surface species and oxalate (oxalic acid) speciation in solution as a function of pH. The fitting was carried out with MatLab 4.2 in conjunction with Acuchem software. The generalized two-layer model was chosen taking into account the oxide surface area, the concentration of the surface sites and the ionic strength of the solution.

Results and discussion

The following results refer to the most important experimental findings obtained during the course of this study.

Degradation of oxalic acid on EGF/Fe(0.4%) fabrics

Fig. 1 shows the mineralization of oxalic acid in the dark and under Suntest light irradiation when the Fenton reagent Fe^{3+}/H_2O_2 is in contact, either in a homogeneous or heterogeneous way, with the oxalic acid solution. It is readily seen that dark runs with 2 mg l^{-1} of Fe(III) or EGF/Fe(0.4%) fabrics do not lead to any oxalic acid mineralization. The EGF/Fe(0.4%) fabric, under light, mediated 80% oxalic degradation in a process that will be shown to involve dual heterogeneous-homogeneous photocatalysis. When Fe^{3+}/H_2O_2 was added homogeneously to the solution containing oxalic acid, 80% of the initial oxalic acid was degraded under light irradiation as shown in Fig. 1. More interesting is the observation in Fig. 1 that an EGF/Fe(0.4%) fabric in the dark is ineffective in oxalic acid abatement. When only H_2O_2 is added, less than 10% of the oxalic acid is degraded under light after 120 min. At each experimental point shown in Fig. 1 the residual H_2O_2 was quenched with bisulfate immediately after the given time to avoid further oxidation of the substrate by H_2O_2. The absence of oxalic acid degradation during the dark reaction (Fig. 1) shows that oxalic acid is unreactive with OH radicals.

Fig. 2(a) shows the mineralization of oxalate at different pH values under Suntest light in a solution with the same make-up as that used to give the results in Fig. 1. The results obtained show that the mineralization mediated by the EGF/Fe(0.4%) fabric proceeds in an acid solution but attains only 50% of the maximum degradation at pH ~3.61. A systematic decrease

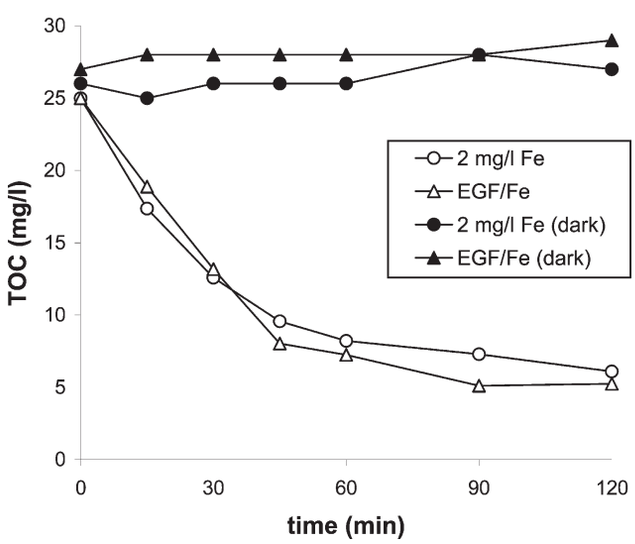

Fig. 1 Mineralization of oxalic acid (1.1 mM) at pH 2.75 under Suntest light irradiation (90 mW cm^{-2}) in a solution containing H_2O_2 (10 mM) using homogeneous Fe ions and EGF/Fe(0.4%) fabric as catalysts. Full symbols refer to dark runs and open symbols refer to light runs.

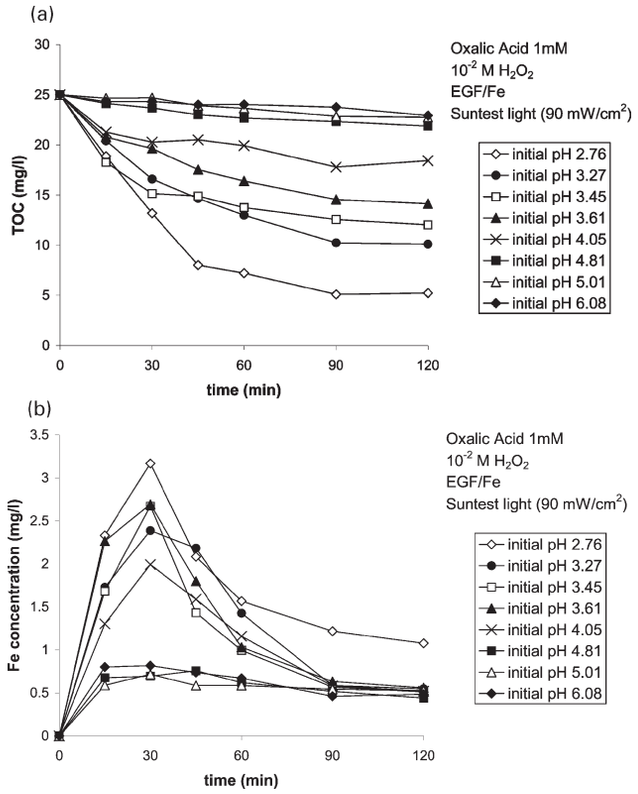

Fig. 2 (a) Mineralization of oxalic acid (1.1 mM) under Suntest light irradiation (86 mW cm^{-2}) and in the dark in a H_2O_2 (10 mM) solution as a function of pH in the presence of an EGF/Fe(0.4%) fabric. (b) Concentration of Fe ions in solution from an EGF/Fe(0.4%) fabric as a function of time during Suntest irradiation of a solution with the same make up as in (a), at different pH values.

in the oxalate mineralization is seen when the reaction is carried out at more basic pH values (pH range 2.76–6.08). Fig. 2(b) shows the profile of the Fe ions available in solution during runs at different pH values under the conditions reported in Fig. 2(a). Fig. 2(b) also shows that the concentration of iron increases with time up to ~30 min and then decreases to around 0.5 mg l^{-1} with the exception of the pH 2.76 solution.

Extent of the homogeneous and heterogeneous catalysis

To assess the extent of the homogeneous catalysis process leading to oxalic acid oxidation, several experiments were performed in homogeneous solution at different concentrations of iron ions and at different pH values. This was to estimate the participation of the homogeneous catalysis in the overall process within the pH range of 2.5–5.5. Table 1 shows the pseudo-first-order rate constants calculated by fitting the degradation results under these experimental conditions. To distinguish the contribution of heterogeneous and homogeneous catalysis during oxalic acid oxidation (steady state), we consider the competing reactions

$$\text{Ox-acid} + H_2O_2 + \text{Fe(OH)}_3\text{/Fe oxide} \rightarrow \text{oxidation products};\ k_{\text{hetero}} \quad (1)$$

$$\text{Ox-acid} + H_2O_2 + Fe^{2+} \rightarrow \text{oxidation products};\ k_{\text{homo}} \quad (2)$$

where k_{hetero} and $k_{\text{homo}}$are the pseudo-first-order rate constants for heterogeneous and homogeneous catalysis, respectively. Therefore, the observed rate constant becomes:

$$k_{\text{obs}} = k_{\text{hetero}} + k_{\text{homo}} \quad (3)$$

The contribution of heterogeneous catalysis (k_{hetero}) can be estimated from eqn. (4) once the rate constant for the homogeneous reactions is known:

$$P_{\text{hetero}} = \frac{k_{\text{hetero}}}{k_{\text{obs}}} \cdot 100 = \frac{k_{\text{obs}} - k_{\text{homo}}}{k_{\text{obs}}} \cdot 100 \quad (4)$$

where P_{hetero} is the percentage of heterogeneous catalysis during the degradation of the oxalates. The k_{homo} values obtained by homogeneous phase experiments with 2 mg L^{-1} of iron were used to identify the contribution of the homogeneous oxidation only since this is the highest concentration of Fe ions released by the EGF/Fe(0.4%) fabric into the solution. This iron concentration was chosen as the reference value for homogeneous degradation as shown in Fig. 1. Table 2 gives the pseudo-first-order rate constants and the percentages of heterogeneous and homogeneous catalysis; the heterogeneous process represents 67% of the overall degradation at pH 3.6 and 93% at pH 5.5. Homogeneous catalysis only plays a dominant role in an acidic medium (68% homogeneous oxidation at pH 2.5).

Fig. 2(b) shows that at the most acidic pH (2.76) about 1 mg l^{-1} of Fe ion is left in solution and a slightly higher degradation of the oxalates is observed with the EGF/Fe(0.4%) fabric as compared to the homogeneous process at the same pH (Fig. 1). This confirms the data presented for the heterogeneous and homogeneous processes in Tables 1 and 2. The release and subsequent re-adsorption of Fe ions [Fig. 2(b)] on the silica fabric explain the accelerating effect introduced by the Fe ions originating from the EGF/Fe(0.4%) fabric.

Formation of oxalate complex(es) on EGF/Fe(0.4%) fabrics

Fig. 3 shows the effect of H_2O_2concentration on the photodegradation of oxalic acid on the EGF/Fe(0.4%) fabrics. The explanation of the most interesting feature in Fig. 3 relates to the decrease observed of TOC in the absence of H_2O_2. This decrease is due to complex formation between oxalic acid and Fe ions. For an initial oxalic acid concentration of 1.1 mM a final concentration of 0.25 mM was measured after adding 10 mM H_2O_2 in the presence of Fe ions at a concentration $\leq$0.05 mM. The oxalic acid is present in a large excess relative to the Fe^{3+} ion concentration and the resulting $[Fe^{3+}\cdots(Ox^{-})_i]$ complexes have high stability constants:[10,13] (a) mono-oxalate with $K_1 = 5.5 \times 10^7$ M^{-1}, (b) $K_2 = 3.4 \times 10^{16}$ M^{-1} and (c) $K_3 = 10^{20}$ M^{-1}. These $[Fe^{3+}\cdots(Ox^{-})_i]$ complexes with $i = 1$, 2, 3 undergo photolysis: $Fe^{III}(Ox)_3^{3-} + h\nu \rightarrow Fe^{III}(Ox)_3^{3-*}$; $Fe^{III}(Ox)_3^{3-*} \rightarrow Fe^{III}(Ox)_2^{2-} + Ox^{\bullet -}$; $Ox^{\bullet -} + Fe^{III}(Ox)_3^{3-} \rightarrow Fe^{III}(Ox)_2^{2-} + 2\ CO_2$; $Fe^{III}(Ox)_3^{3-*} \rightarrow$ quenching. These latter

Table 1 Total iron concentrations and pseudo-first-order rate constants for the oxidation of oxalate acid under different pH values

pH	C_{Fe}/mg L^{-1}	k_{homo}/s^{-1}
2.5	2	2.42×10^{-4}
	3	2.33×10^{-4}
	5	2.28×10^{-4}
3.6	2	3.42×10^{-5}
	3	4.68×10^{-5}
	5	5.50×10^{-5}
5.5	2	9.40×10^{-7}
	3	1.19×10^{-5}
	5	1.51×10^{-5}

Table 2 Pseudo-first-order rate constants and percentage of homogeneous and heterogeneous catalysis for the oxidation of oxalates under different pH values

pH	k_{obs}/s^{-1}	k_{homo}/s^{-1}	k_{hetero}/s^{-1}	% P_{homo}	% P_{hetero}
2.5	3.53×10^{-4}	2.42×10^{-4}	1.12×10^{-4}	68	32
3.6	1.02×10^{-4}	3.42×10^{-5}	6.83×10^{-5}	33	67
5.5	1.26×10^{-5}	9.40×10^{-7}	1.16×10^{-5}	7	93

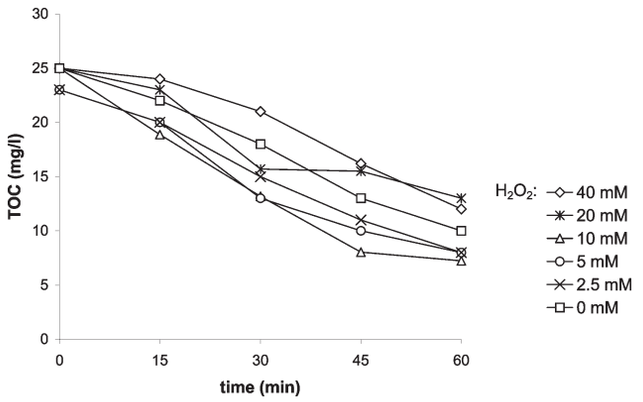

Fig. 3 Mineralization of oxalic acid (1.1 mM) under Suntest light irradiation (90 mW cm^{-2}) as a function of H_2O_2 concentration at pH 2.75 in the presence of an EGF/Fe(0.4%) fabric.

reactions explain the TOC decrease in the absence of H_2O_2. Because the solution concentration of Fe^{3+} is much less than that of oxalic acid, the TOC decrease in the absence of H_2O_2 cannot be explained by homogeneous reactions. Since the recovery of Fe(II) to Fe(III) is slow in the presence of air (as known from ferrioxalate actinometry[4,9]), the oxidation of oxalic acid due to photolysis in solution is not sufficient and cannot explain the observed kinetics. Therefore, the surface-bound Fe(III) has to be taken into account and the addition of H_2O_2 accelerates the recovery of Fe(II) to Fe(III) through the reaction

$$Fe^{2+} + H_2O_2 \rightarrow Fe^{3+} + OH^{\bullet} + OH^{-} \qquad (5)$$

and this in turn increases the concentration of the complex $[Fe^{3+}\cdots(Ox^{-})_i]$ accelerating the rate of oxalate degradation due to photolysis.

Fig. 3 shows that an increase in the hydrogen peroxide concentration above 10 mM leads to a decrease of the oxalic acid degradation rate. The two factors involved in the decrease at higher H_2O_2 concentrations are the well-known scavenging of $OH^{\bullet}$ by excess H_2O_2:

$$H_2O_2 + OH^{\circ} \rightarrow HO_2^{\circ} + H_2O; \quad k_6 = 2.7 \times 10^7\ M^{-1}\ s^{-1} \qquad (6)$$

and the quenching of $Fe^{III}(Ox)_3^{3-}*$ by the peroxide:[13]

$$Fe^{III}(Ox)_3^{3-}* + H_2O_2 \rightarrow \text{quenching} \qquad (7)$$

Taking α as a constant directly proportional to the absorption coefficient and quantum yield of the $[Fe^{3+}\cdots(Ox^{-})_i]$ complex dissociation, it can be seen from eqn. (8) that the variation of TOC degradation as a function of H_2O_2 concentration has kinetics showing first an increase and later a decrease:[4,9,10,14]

$$\frac{d[Ox^{2-}]}{dt} \approx \frac{\alpha I}{\frac{1}{\tau} + K_q[H_2O_2]} + \frac{k_5 k_6 [Fe(II)][Ox][H_2O_2]}{k_6[Ox^{2-}] + k_7[H_2O_2]} \qquad (8)$$

Degradation of oxalates in acid solutions mediated by an EGF/Fe(0.4%) fabric. Surface interactions

Fig. 4 presents the catalytic nature of the catalyzed oxalate photodegradation under Suntest light irradiation on EGF/Fe(0.4%) fabrics in the presence of H_2O_2. At the end of each degradation cycle, the initial amounts of oxalate and H_2O_2 were added to the original solution and the photodegradation cycle started again. The amount of Fe ions found corresponds to the amount present after 60 min irradiation as reported previously in Fig. 2(b). After each cycle in Fig. 4, the same amount of Fe ions was released into the solution.

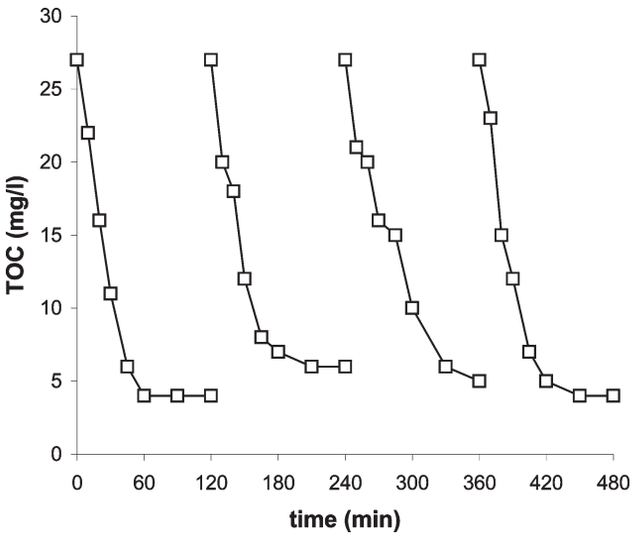

Fig. 4 Repetitive photocatalytic mineralization of oxalic acid (1 mM) on an EGF/Fe(0.4%) fabric under Suntest light irradiation in the presence of H_2O_2 (10 mM) at pH 2.75.

To understand the interaction between the hematite cluster on the silica fabric and the oxalates in solution, the speciation of hematite in solution is composed of four species:[14,15] $\equiv FeOH_2^{+}$, $\equiv FeOH$, $\equiv FeO^{-}$ and $\equiv FeL$, where $\equiv FeL$ denotes the surface complex ligand for oxalates, H_2L denotes oxalic acid, L^{2-} refers to the oxalate and the initial concentration of the oxalate equals $H_2L + HL^{-} + L^{2-}$. The equations in Table 3 represent the equilibria between the species due to the surface protonation as a function of pH.

Infrared characterization of Fe carboxylates during oxalate photodegradation

Fig. 5 shows the existence of Fe carboxylate intermediates during the EGF/Fe(0.4%) mediated photodegradation of oxalic acid. Fig. 5(a) shows the attenuated total reflection infrared spectra (ATRIR) of EGF/Fe(0.4%) fabrics after adsorption of different concentrations of oxalic acid. The spectra present Fe oxalate surface complexes and their disappearance during the photodegradation process. In Fig. 5(a), the band at 1740 cm^{-1} is characteristic of a bidentate coordination carboxyl group ($-COO^{-}$) for an oxalic acid group adsorbed onto the fabric and corresponds to a $Fe(Ox)_3^{3-}$ surface complex. An additional lower wavenumber shoulder observed around 1650 cm^{-1} also gives evidence for the formation of the $Fe(Ox)_3^{3-}$ surface complex; it is also the evidence for small amounts of a $Fe(Ox)_2^{2-}$ surface complex. The strong band at 1630 cm^{-1} due to the bending vibration of the OH group does not allow us to estimate the amount of $Fe(Ox)_2^{2-}$. The $Fe(Ox)_3^{3-}$ with three oxalic groups has a tri-dimensional structure in solution.[1,10,16] When iron oxalate equilibrates at the silica surface there is not enough space to accommodate the tri-dimensional structure. Therefore, a shift in the band

Table 3 Equilibrium expressions and mass balance equations for surface complexation reactions

$\equiv FeOH_2^{+} \Leftrightarrow \equiv FeOH + H^{+}$	$\log K_{a1} = -6.7$
$\equiv FeOH \Leftrightarrow \equiv FeO^{-} + H^{+}$	$\log K_{a2} = -10.4$
$\equiv FeOH + HL^{-} \Leftrightarrow \equiv FeL^{-} + H_2O$	$\log K_L$
$H_2L \Leftrightarrow HL^{-} + H^{+}$	$\log K_{H2L} = -1.23$
$HL^{-} \Leftrightarrow L^{2-} + H^{+}$	$\log K_{HL} = -4.19$
$S_T = [\equiv FeOH_2^{+}] + [\equiv FeOH] + [\equiv FeO^{-}] + [\equiv FeL^{-}]$	
$OxA_T = [H_2L] + [HL^{-}] + [L^{2-}] + [\equiv FeL^{-}]$	

H_2L, oxalic acid; L^{2-}, oxalate; $C_{OxA} = H_2L + HL^{-} + L^{2-}$

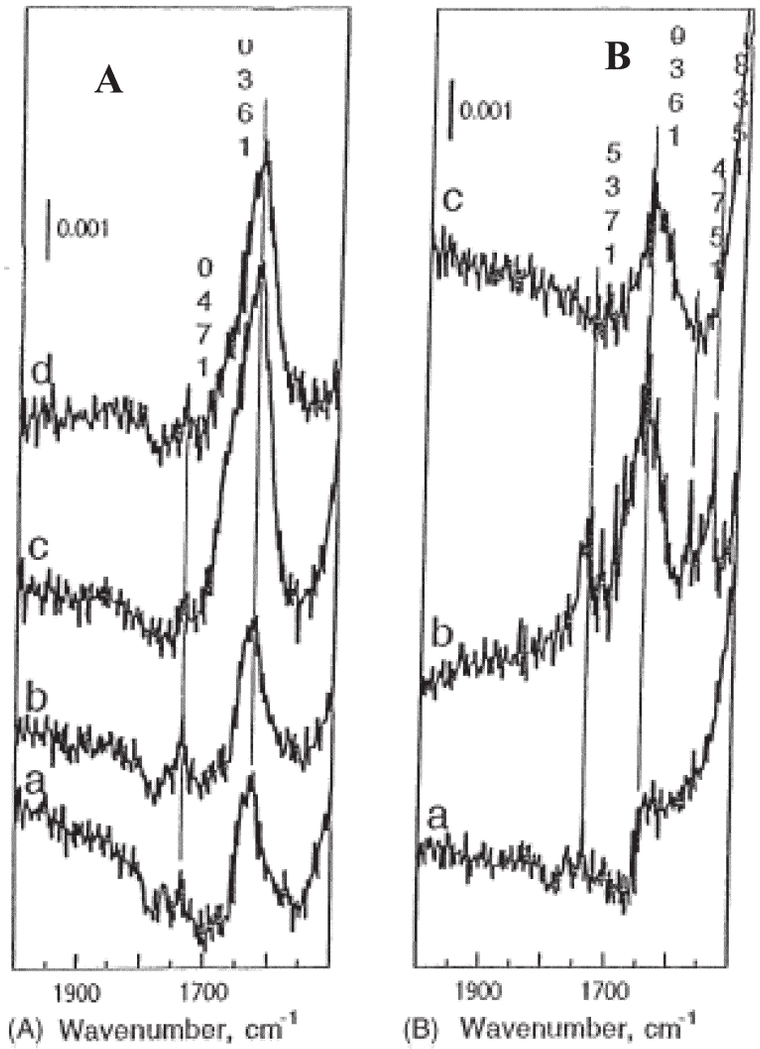

Fig. 5 (a) ATRIR spectra of an EGF/Fe(0.4%) silica fabric equilibrated with different concentrations of oxalates at pH 2.75: (a) 0.1, (b) 1, (c) 2 and (d) 5 mM. (b) ATRIR spectra of an EGF/Fe(0.4%) silica fabric during Suntest irradiation of a solution of oxalate (1.1 mM) containing H_2O_2 (10 mM) at pH 2.75: (a) 0, (b) 15 and (c) 60 min.

positions is observed when surface and bulk precipitated $Fe(Ox)_3^{3-}$ complexes are compared.[17,18]

Fig. 5(b) shows the adsorption, at zero time and after 15 min, of the carboxylate groups at 1735 and 1623 cm^{-1} and the asymmetric stretching vibration doublet at 1574 and 1538 cm^{-1}. This clearly indicates the formation of the $Fe(Ox)_3^{3-}$ surface complex with the bidentate carboxyl group of oxalate. After 15 min, a maximum in the Fe carboxylate band is observed and only a trace of the initial caboxylate is found on the surface. After 60 min, the bands originating from either carboxylic non-coordinated groups or Fe carboxylate complexes have disappeared. The IR bands at 1740 and 1630 cm^{-1} in Fig. 5(a) are shifted in Fig. 5(b) to 1735 and 1623 cm^{-1}, respectively, due to H-bonding when carboxyl groups are transformed into carboxylate groups on the silica fabric.[16,17] Another interesting observation is that iron loading increases the number of surface OH groups found in the 3200–3500 cm^{-1} region. After 30–45 min the number of OH groups was observed to be constant. Strong bands at 1066 and 888 cm^{-1} due to the SiO_2 stretching vibration of the fabric overlap with OH and Fe–O bands. In addition, a good contrast was not obtained in the IR spectra of the EGF/Fe(0.4%) fabrics since these samples are fibrous and homogeneous radiation is not possible on these surfaces.

No spectroscopic evidence by ATRIR was found for the presence of the iron oxalate surface complex on fabrics pre-equilibrated with oxalic acid and irradiated subsequently for 5, 10, 20, 30 and 60 min. The results show that no carboxylate species were formed during oxalate degradation on fabrics having only surface [–Si–O–] species.

Nature of the iron species on the surface of the EGF/Fe(0.4%) fabric

IR spectra (Fig. 6) also give no spectroscopic evidence for the presence of the iron oxalate surface complex on the EGF/Fe(0.4%) fabric pre-equilibrated in oxalate (1 mM) solution and subsequently irradiated as described above. The EGF/Fe(0.4%) fabric was equilibrated overnight before use with oxalic acid to eliminate the Fe oxide species (–Fe–O–Fe–). The results show that no carboxylate species are formed during oxalic acid degradation on fabrics where only (–Si–O–Fe–) catalytic clusters are available on the catalyst surface. It is readily seen in Fig. 7 that in a leached fabric the degradation of oxalates is considerably decreased with respect to non-leached materials, pointing to the lower photocatalytic activity of the (–Si–O–Fe–) clusters.

Suggested mineralization mechanism of oxalates mediated by the EGF/Fe(0.4%) fabric

Scheme 1 is suggested as the photodegradation pathway for oxalates, consistent with the results presented in Figs. 1–5. The EGF/Fe(0.4%) fabric acts as a sink for the oxalate in

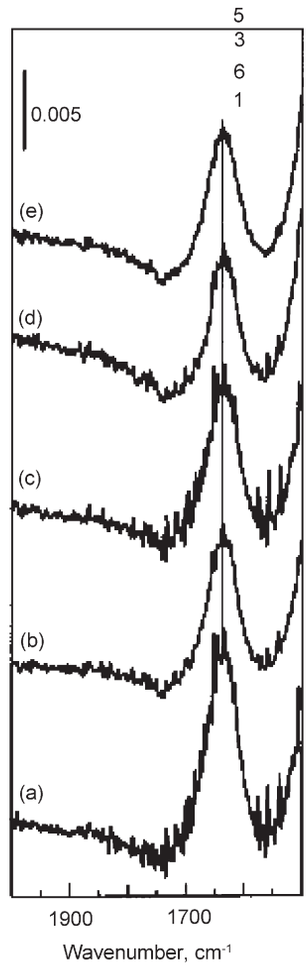

Fig. 6 IR spectra of EGF/Fe(0.4%) silica fabric during Suntest irradiation of a solution of oxalic acid (1.0 mM) containing H_2O_2 (10 mM) at pH 2.75 irradiated for (a) 5, (b) 10, (c) 20, (d) 30 and (e) 60 min. The EGF/Fe(0.4%) silica fabric had been equilibrated before use in the dark with oxalic acid (1.0 mM).

solution in a reaction where the iron acts as a heterogeneous catalyst and reacts with the oxalate ions in solution: $Fe_{hetero} + ox^{-2} \Leftrightarrow Fe(Ox^{-2})_{homo}^{+}$. The latter Fe omplex can subsequently add two more oxalate groups to form $Fe(Ox)_3^{-3}$,

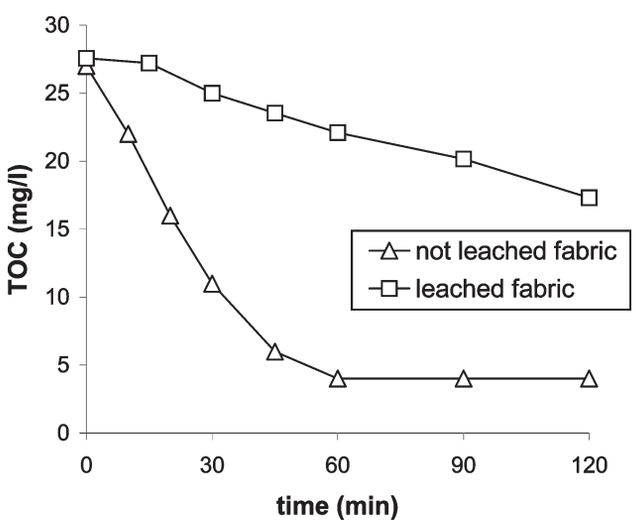

Fig. 7 Mineralization of oxalic acid (1.1 mM) on an EGF/Fe(0.4%) fabric under Suntest light irradiation (90 mW cm^{-2}) in the presence of H_2O_2 (10 mM) at pH 2.75 before equilibration and after equilibration for 16 h in oxalic acid (1.0 M) in the dark.

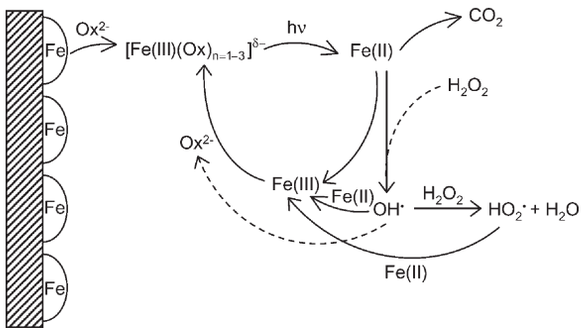

Scheme 1

the initial dominant complex in solution. The absorption of a photon by an Fe(III) oxalate complex results in an electron transfer from a complexing oxalate ligand to the Fe(III) ion, producing a ferrous ion and an oxalate radical anion. The LMCT photo-decarboxylation of the Fe oxalate complex (Fig. 1) is a fairly common process,[9,19] resulting in the reduction of Fe(III) and evolution of CO_2. As the abatement of oxalate progresses (see Figs. 1 and 2) the TOC decreases due to the depletion of the Fe oxalate and consumption of oxalic acid in solution. Since at longer reaction times less $[Fe(III)(Ox)_{n\,=\,1\text{–}3}]^{\delta-}$ is available to the solution, it follows that the concentration of Fe(II) also decreases with time as shown by the decrease in Fe(II) concentration in Fig. 2(b). The hydroxyl and superoxyide radicals noted in Scheme 1 become available due to the added H_2O_2 in the presence of Fe(III)/Fe(II) ions under light irradiation and interact in a series of consecutive reactions leading to oxalate mineralization.

By estimating the encounter-pair time for the four main reactions following $[Fe(III)(Ox)_{n\,=\,1\text{–}3}]^{\delta-}$ decomposition under light in the presence of H_2O_2 (10 mM), the $OH^{\bullet}$ formation or consumption probability can be estimated in Scheme 1 from the reciprocal of the encounter-pair lifetime of the reactions: (a) $OH^{\bullet} + (Ox^{2-}) \rightarrow OH^{-} + Ox^{-\bullet}$, with $k = 2 \times 10^6$ M^{-1} s^{-1} and $[Ox^{2-}] = 10^{-3}$ M, gives a value for the reciprocal encounter-pair lifetime of $\sim 2 \times 10^3$ s^{-1}; (b) $OH^{\bullet} + Fe^{2+} \rightarrow OH^{-} + Fe^{3+}$, with $k = 3 \times 10^8$ M^{-1} s^{-1} and $[Fe^{2+}] = 7 \times 10^{-5}$ M, the latter value is $\sim 2.1 \times 10^4$ s^{-1}; (c) $OH^{\bullet} + H_2O_2 \rightarrow HO_2^{\bullet} + H_2O$, with $k = 1.3 \times 10^7$ M^{-1} s^{-1} and $[H_2O_2] = 10^{-2}$ M, the latter value is $\sim 1.3 \times 10^5$ s^{-1}; and finally, (d) $H_2O_2 + Fe^{2+} \rightarrow OH^{\bullet} + OH^{-} + Fe^{3+}$, with $k = 47$ M^{-1} s^{-1} and $[H_2O_2] = 10^{-2}$ M, the latter value is ~ 0.47 s^{-1}. From reactions (a)–(c) above the radical $OH^{\bullet}$ is mainly consumed by H_2O_2 and not formed by the reaction (c) in Scheme 1 since 1.3×10^5 s$^{-1} \gg 0.47$ s^{-1}. Also it can be estimated that the $OH^{\bullet}$ radical is consumed by reaction (c) and not by reaction (a) since 1.3×10^5 s$^{-1} > 2.3 \times 10^3$ s^{-1} indicating that only 1% of the $OH^{\bullet}$ radical reacts with oxalic acid in the presence of H_2O_2 (10 mM). The main decomposition channel of oxalate involves a Fe carboxylate redox process (see Fig. 3): $[RCO_2\text{–}Fe]^{2+} \rightarrow [R^{\bullet}] + CO_2 + Fe^{2+}$. Analysis of the amount of Fe extracted from the surface due to oxalate varies between 0.1% and 0.2% of the total Fe available. XPS results confirmed that the depletion of Fe on the fabric increased with the time and concentration of oxalic acid used. The iron remaining on the EFG/Fe(0.4%) fabric surface acts as crystallization nuclei for the Fe ions returning from the solution, due to the overbearing presence of the Fe-loaded fabric in the system under study.[5,10,13,14]

Transmission electron microscopy (HRTEM) studies

Fig. 7 shows that leaching out the hematite on the catalyst surface with oxalic acid (1 M) for 16 h leads to the mineralization of oxalic acid with a slower rate due to the remaining (–Si–O–Fe–) on the silica fabric. The leaching process was carried out

by equilibrating the EGF/Fe(0.4%) fabric overnight with oxalic acid to eliminate the Fe oxide species (–Fe–O–Fe–). Fig. 8(a), obtained by HRTEM, shows Fe clusters with ≤1 nm size (centered around 0.4 nm) distributed on the silica fabric. The Fe clusters are seen with a fairly homogeneous dispersion on the lower left hand side of Fig. 8(a). Fig. 8(b) shows the characterization of the EGF/Fe(0.4%) fabric surface using EDX additionally to HRTEM measurements. The (–Si–O–Fe–) species formation takes place during catalyst calcination at 450 °C and is present as a layer 0.147 μm thick. These observations confirm the presence of one active catalytic iron species (–Fe–O–Fe–) and another less active species (–Si–O–Fe–) on the EGF/Fe(0.4%) fabric.

XPS analysis of EGF/Fe(0.4%) fabric

XPS spectroscopy was used to further characterize the EGF/Fe(0.4%) fabric before and after reaction. The referencing and correction of the Fe -peaks observed by X-ray photoelectron spectroscopy was carried out as reported recently by our laboratory.[11] Table 4 reports the percentage coverage for the elements found on the silica surface carried out according to DIN[20] by comparing with known spectra of silica. The measurements had an error margin of 5%. The surface C seems to be removed during the preparation of the Fe-loaded silica fabric. The surface fluorine is seen to increase due to the migration of the F in the fabric during the calcination step. The Fe present represents more than 5% of the surface area

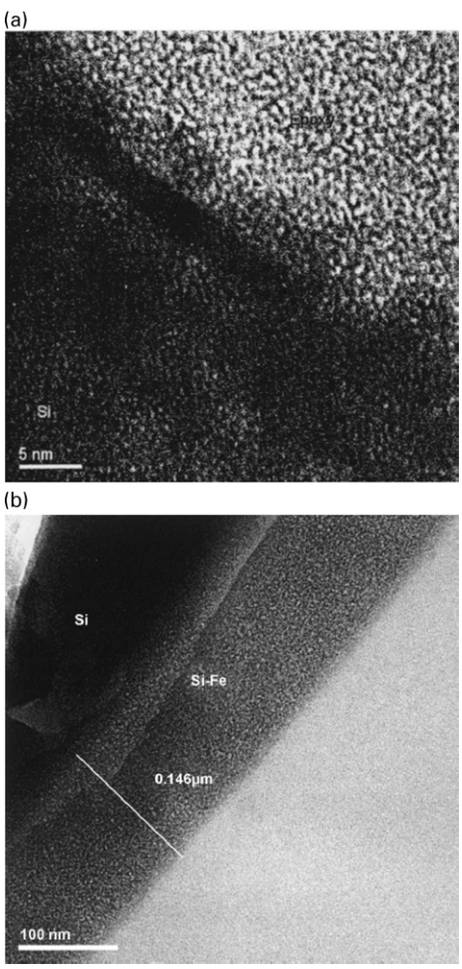

Fig. 8 (a) High resolution electron microscopy (HRTEM) showing the Fe cluster on the silica fabric surface. (b) High resolution electron microscopy (HRTEM) of the silica fabric showing the interfacial Fe silicate identified by means of electron dispersive X-ray spectrometry (EDX).

Table 4 Elemental analysis by XPS of silica and EGF/Fe fabrics

Element peak	Silica fabric	EGF/Fe fabric
C 1s	26	12.7
N 1s	0.75	0.42
O 1s	43	51.3
F 1s	0.75	2.25
Al 2p	1.48	2.01
Si 2p	27.5	22.6
Ca 2p	0.47	3.29
Fe 2p	<0.1	5.06

of the fabric as seen in the last row in Table 4. This is a surprisingly high value. The fabric is highly loaded with iron and acts as a *reservoir* of Fe(III) that replenishes Fe^{3+} in solution as it is photoreduced during the course of the reaction.

From the binding energies (BE) in Table 5, the Fe_{2p} doublet is seen to shift slightly after the photocatalytic process on the EGF/Fe(0.4%) fabric. This is indicative of a small reduction from the Fe(III) to the Fe(II) state of the iron after the EGF/Fe(0.4%)fabric has been used during the degradation of oxalic acid. This is confirmed by the fading of the pale orange color of the fabrics to yellow after use since FeO/Fe(II) is colorless. The XPS signal observed at 708.9 eV is ascribed to Fe(II) and at 711.2 eV to Fe(III). The peak observed at 713.4 eV originates from the peak asymmetry observed in the Fe oxide band envelope (FeO/Fe_2O_3).

Gas adsorption, porosity and BET measurements

Table 6 shows the specific surface area and the BJH[21] desorption pore diameter, total pore volume and average pore diameter at zero time and after 2 h for light-induced processes during oxalate degradation with an EGF/Fe(0.4%) fabric. BET analysis showed that the surface area of the fabrics increased modestly after oxalate abatement. By using the Barret, Joyner and Halenda (BJH) model, a desorption pore diameter of ~38 Å could be estimated for the SiO_2 fabric before and after use. The values obtained point to the stability of the fabric during oxalate abatement.

Conclusions

This study presents an innovative Fenton immobilized catalyst consisting of iron oxide silica fabrics able to efficiently oxidize

Table 5 Binding energies of the Fe ion in EGF/Fe fabric

	Before use		After use	
Spectral peak	BE/eV	%	BE/eV	%
Fe $2p_{3/2}$	708.9	0.01	708.8	0.03
Fe $2p_{3/2}$ox	711.2	59.6	710.9	57.8
Fe $2p_{3/2}$ox'	713.4	40.4	713.0	42.2

Table 6 Surface adsorption of the EGF/Fe fabric

	Zero time	After 2 h
BET surface area/m^2 g^{-1}	9.8	13.4
BJH desorption pore diameter/Å	37.2	38.3
Average pore diameter/Å	32.9	26.3
Pore volume/cm^3 g^{-1}	0.0085	0.0088

organic compounds such as oxalic acid and oxalates. The mechanism involved is quite complex since it involves two Fe redox states driving the conversion of the oxalate by using up the H_2O_2 added as oxidant. The photoreduction of Fe(III) oxalate complexes is shown to play an important part in the overall decomposition of oxalate as opposed to the mechanism with solution phase complexes. At pH values >3.6 heterogeneous catalysis plays the major role during the photocatalytic degradation of oxalates on EGF/(Fe(0.4%) fabrics. The Fe ions fixed on the silica fabric form surface complexes of the type Fe(II)/(III)–R that are photosensitive, leading to electron transfer reactions. Evidence is provided for the degradation of oxalic acid oxalates on the Fe–silica fabric due to Fe ions leaching into the solution and being re-adsorbed onto the silica fabric. The decomposition of the Fe carboxylates under light is shown to have the triple benefit of (a) reducing the TOC in solution, (b) forming Fe^{2+} ions that can be reused in the initial Fenton reaction and (c) liberating organic radicals that subsequently oxidize the organic intermediates in solution. Two types of iron speciation were found on the silica surface with a specific mode of intervention during the abatement of oxalates.

Acknowledgements

We gratefully acknowledge the partial support for this work by KTI/CTI TOP NANO 21 (Bern, Switzerland) under Grant N° 6116.4 TNS and of COST D19 program under Grant N° CO2.0068. We thank P. A. Buffat and D. Laub for their help with the electron microscopy measurements.

References

1 R. Mehrotra and R. Bohra, *Metal Carboxylates*, Academic Press, London, 1983.
2 R. Hoffmann, *Angew. Chem.*, 1987, **99**, 871.
3 L. Kiwi-Minsker, J. Yuranov, E. Slavinskaia, V. Zaikovski and A. Renken, *Catal. Today*, 2000, **59**, 61.
4 M. Halmann, *Photodegradation of Water Pollutants*, CRC Publishing Co., Boca Raton Fl, 1976.
5 J. Fernandez, J. Bandara, A. Lopez, P. A. Buffat and J. Kiwi, *Langmuir*, 1999, **15**, 185.
6 R. Watts, S. Kong, M. Orr and G. Miller, *Environ. Technol.*, 1994, **15**, 469.
7 K. Nam, W. Todriguez and J. Kukor, *Chemosphere*, 2001, **45**, 11.
8 *EEC List of Council Directives 76/4647*, European Economic Community, Brussels, 1976.
9 C. G. Hatchard and A. Parker, *Proc. R. Soc. London, Ser. A*, 1956, **235**, 518.
10 V. Nadtochenko and J. Kiwi, *J. Chem. Soc., Faraday Trans.*, 1997, **93**, 2373.
11 N. J. Harrick, *Internal Reflection Spectroscopy*, Harrick Science Co., Ossining, New York, 1987.
12 A. Shirley, *Phys. Rev.*, 1979, **135**, 4709.
13 V. Nadtochenko and J. Kiwi, *J. Photochem. Photobiol., A.*, 1996, **99**, 145.
14 W. Stumm and J. Morgan, *Aquatic Chemistry*, Wiley Interscience, New York, 1997.
15 Y. Zuo and J. Hoigné, *Environ. Sci. Technol.*, 1992, **26**, 1014.
16 A. Sima and S. Makanova, *J. Coord. Chem. Rev.*, 1997, **160**, 161.
17 L. Bellamy, *Infrared Spectra of Complex Molecules*, Chapman and Hall, New York, 1985.
18 M. Edwards and C. Russell, *J. Mol. Struct.*, 1998, **470**, 223.
19 S. Banwart, S. Davies and W. Stumm, *Colloids Surf.*, 1989, **39**, 303.
20 *Norms of the National Physics Laboratory*, Section: Surfaces and Microanalysis, DIN 39 and DIN NMP 816, Teddington, UK. .
21 P. Barret, L. Joyner and P. Halenda, *J. Am. Chem. Soc.*, 1951, **73**, 1371.